Journal of Alloys and Compounds 506 (2010) 559–564

Contents lists available at ScienceDirect

Journal of Alloys and Compounds

journal homepage: www.elsevier.com/locate/jallcom

Electrochemical characteristics of AB_5-type hydrogen storage alloys

M. Tliha[a,*], S. Boussami[a], H. Mathlouthi[a], J. Lamloumi[a], A. Percheron-Guégan[b]

[a] Laboratoire de Mécanique, Matériaux et Procédés, ESSTT, 5 Avenue Taha Hussein 1008 Tunis, Tunisia
[b] Laboratoire de Chimie Métallurgique des Terres Rares, GLVT, 2-8 Rue Henri Dunant 94320, Thiais Cedex, France

ARTICLE INFO

Article history:
Received 25 May 2010
Received in revised form 1 July 2010
Accepted 7 July 2010
Available online 15 July 2010

Keywords:
Hydrogen insertion
Electrochemical kinetic
Hydrogen absorbing materials
Exchange current density
State of charge

ABSTRACT

The kinetic behaviour of the $LaNi_{3.55}Mn_{0.4}Al_{0.3}Co_{0.4}Fe_{0.35}$ metal hydride, used as a negative electrode in the nickel/metal-hydride (Ni/MH) batteries, was investigated using electrochemical impedance spectroscopy (EIS) at different state of charge (SOC). Impedance measurements were performed in the frequency range from 50 kHz to 1 mHz. Electrochemical impedance spectrum of the metal hydride electrode was interpreted by an equivalent circuit including the different electrochemical processes taking place on the interface between the MH electrode and the electrolyte. Electrochemical kinetic parameters such as the charge-transfer resistance R_{tc}, the exchange current density I_0 and the hydrogen diffusion coefficient D_H were determined at different state of charge. The results of EIS measurements indicate that the electrochemical reaction activity of the $LaNi_{3.55}Mn_{0.4}Al_{0.3}Co_{0.4}Fe_{0.35}$ metal hydride electrode was markedly improved with increasing state of charge (SOC). The transformation α–β is probably a limiting step in the mechanisms of hydrogenation of metal hydride electrode.

1. Introduction

Recently, nickel–metal hydride (Ni–MH) batteries have been developed and commercialized because of their higher energy density, high rate dischargeability, long cycle life, no memory effect and environment cleanness compared with nickel–cadmium (Ni–Cd) batteries. AB_5 hydrogen storage alloys have now been widely used as negative electrode (anode) materials for Ni–MH rechargeable batteries. Much research has been performed in order to improve the overall properties of the AB_5 alloys and to develop new types of alloy electrodes, used as the negative electrode materials of the Ni/MH battery [1–11]. The performance of these electrodes is determined by both the kinetics of the processes occurring at the metal/solution interface and the rate of hydrogen diffusion within the bulk of the metal alloy particles. Different electrochemical methods have been used to study the kinetics process in the hydrogen storage alloys [12–15]. Electrochemical impedance spectroscopy (EIS) is a powerful analysis technique, which can provide a wealth of information on the corrosion reactions, the mass transport and the electrical charge transfer characteristics of the electrode/solution interface.

In this paper, the electrochemical impedance characteristics of the $LaNi_{3.55}Mn_{0.4}Al_{0.3}Co_{0.4}Fe_{0.35}$ metal hydride electrode with different state of charge are extensively investigated. The relationship between the parameters of the equivalent circuit elements and the state of charge is discussed.

2. Experimental

The intermetallic compound $LaNi_{3.55}Mn_{0.4}Al_{0.3}Co_{0.4}Fe_{0.35}$ was prepared, by the induction melting of the pure elements followed by an appropriate annealing to ensure a good homogeneity, as reported in Ref. [16]. The $LaNi_{3.55}Mn_{0.4}Al_{0.3}Co_{0.4}Fe_{0.35}$ obtained alloy was first ground and sieved (to less than 63 μm) in a glove box under an argon atmosphere. The so-called "latex" technology has been used for the electrode preparation [17]. Ninety percent of this powder has been mixed with 5% of the polytetrafluorethylene (PTFE) and 5% of the carbon black. The mixture (~0.06 g) was compressed on the two faces of a nickel grid ($S = 0.5\ cm^2$), playing the role of a current collector. The thickness of this electrode is 0.5 mm. The electrochemical measurements were performed at a room temperature in a three-electrode open cell using a Voltalab 40 system (Radiometer Analytical) constituted by a Potentiostat–Galvanostat PGZ301. The MH electrode used as the working electrode, a wire of gold and a Hg/HgO electrode were used as the counter electrode and reference electrode, respectively. The electrolyte consisted of a 7 M KOH solution in which a continuous flow of Ar is kept through the cell.

Electrochemical impedance spectroscopy (EIS) studies were conducted at different state of charge (SOC). Before EIS measurements, the electrode was first completely activated by charging/discharging for 25 cycles. The EIS spectra of the electrode were measured in the frequency range from 50 kHz to 5 mHz with an ac amplitude perturbation of 5 mV under the open-circuit conditions. The EIS measurements were performed only after the open-circuit potential (i.e. equilibrium potential) was stabilized (i.e. a variation in the potential was less than 1 mV for a period of 1 h). EIS spectra were fitted to equivalent circuit using the software ZSimpWin 3.1.

3. Results and discussion

The electrochemical reactions taking place at the electrode/electrolyte interface inside each electrode during charging and discharging can be represented as follows:

$$M + H_2O + e^- \leftrightarrow MH_{ads} + OH^- \quad (1)$$

* Corresponding author. Tel.: +216 71391166; fax: +216 71496066.
E-mail address: Mohamed.Tliha@esstt.rnu.tn (M. Tliha).

0925-8388/$ – see front matter © 2010 Elsevier B.V. All rights reserved.
doi:10.1016/j.jallcom.2010.07.068

$$MH_{ads} \leftrightarrow MH_{abs} \quad (2)$$

$$MH_{abs} \leftrightarrow MH_{hyd} \quad (3)$$

where M is the hydrogen storage alloy, H_{ads} the adsorbed hydrogen on the surface of the alloy, H_{abs} the absorbed hydrogen in the bulk, and H_{hyd} is the metal hydride [18,19]. Reaction (1) reflects the charge-transfer process at the interface between the MH alloy powder and the electrolyte, Reaction (2) is transfer from adsorbed to absorbed state and Reaction (3) represents the diffusion of hydrogen from the surface to the bulk. The performance of the negative electrode is mainly controlled by the kinetics of the hydrogen diffusion process and/or the reactions taking place on the alloy surface. Electrochemical impedance spectroscopy (EIS) is a powerful tool in such a context as it allows to get an understanding of the different processes if their time constants are well separated.

Fig. 1 shows the equilibrium potential of the $LaNi_{3.55}Mn_{0.4}Al_{0.3}Co_{0.4}Fe_{0.35}$ metal hydride alloy electrode at different state of charge. Two regions could be distinguished on this figure. It can be seen when the state of charge of the electrode is less than 40%, the equilibrium potential depends strongly on the hydrogen content. This region corresponds to the single-phase solid solution, called α-phase. Increasing the hydrogen content in the electrode, the equilibrium potential reaches a plateau. This plateau region indicates the formation of β-phase (hydride phase) and at this region two phases (α and β) coexist.

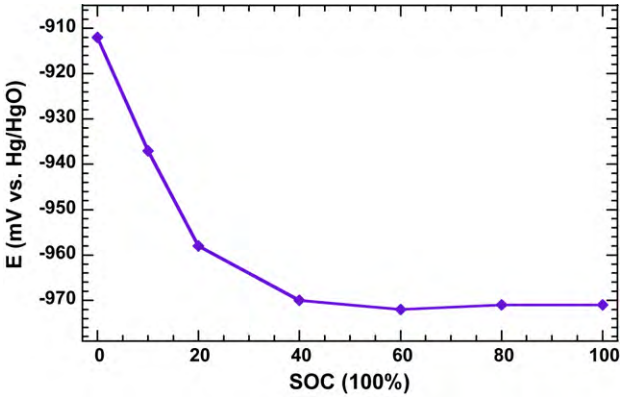

Fig. 1. The equilibrium potential of the $LaNi_{3.55}Mn_{0.4}Al_{0.3}Co_{0.4}Fe_{0.35}$ alloy electrode as a function of the state of charge.

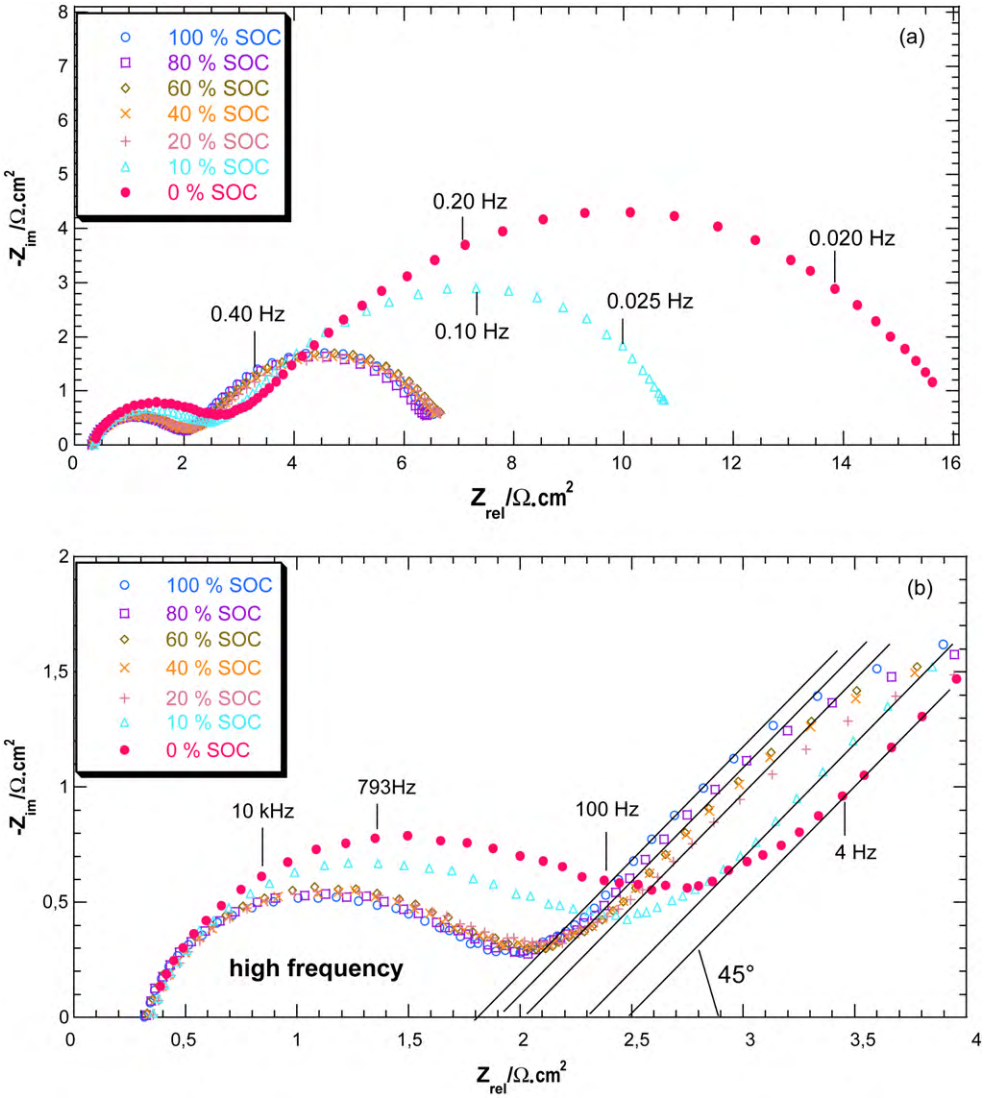

Fig. 2. (a) Nyquist plots of the $LaNi_{3.55}Mn_{0.4}Al_{0.3}Co_{0.4}Fe_{0.35}$ electrode at different state of charge. (b) Enlarged view of the smaller semicircle in the high-frequency region for the $LaNi_{3.55}Mn_{0.4}Al_{0.3}Co_{0.4}Fe_{0.35}$ metal hydride electrode at different state of charge.

The impedance spectroscopy of the $LaNi_{3.55}Mn_{0.4}Al_{0.3}Co_{0.4}Fe_{0.35}$ metal hydride electrode after activation was given in Fig. 2(a) and (b) at different state of charge (SOC). It can be seen that each EIS spectrum consists of a smaller semicircle in the high-frequency region (50 kHz to 20 Hz), a straight line with the angle of about 45° in the middle-frequency region (20–1 Hz) and a larger semicircle in the low-frequency region (1 Hz to 1 mHz). The high-frequency region semicircle can be attributed to the charge transfer process which takes place at interface [20–22], the straight line with the angle of about 45° in the middle-frequency region is attributed to the Warburg diffusion for semi-infinite diffusion [22–25] and the low-frequency region semicircle should be related to the phase transition process (α to β); the hydrogen moving from the alloy's surface to the alloy's bulk, i.e. the conversion of the hydrogen from adsorptive state to absorptive sate, simultaneously accomplished by the phase transition.

The software ZSimpWin 3.1 was used to develop a circuit model from the spectroscopy data. The modeling process was iterative, using the Chi-square (χ^2) value for the entire model and the percent error values for each circuit component to determine the fit of a given model to the experimental data. The χ^2 value was calculated according to the following algorithm:

3.1. Data points and parameters

1. Experimental data point (*frequency*, Z_{real}, Z_{img}) [ω_i, a_i, b_i]
2. Parameters associated with model, $\overline{p} = (p_1, p_2, p_3, \ldots, p_m)$
3. Calculated point, [ω_i, $Z'(\omega_i, \overline{p})$, $Z''(\omega_i, \overline{p})$]
4. Weighting factors, ω_i, W_i', W_i''

3.2. Application of statistics

The distance between exp. and cal. points,

$$d_i^2 = (a_i - Z'(\omega_i;\overline{p}))^2 + (b_i - Z''(\omega_i;\overline{p}))^2$$

The goodness of fit to model,

$$\chi^2 = \sum_{i=1}^{n} [W_i'.(Z_i'(\omega_i;\overline{p}) - a_i)^2 + W_i''.(Z_i''(\omega_i;\overline{p}) - b_i)^2],$$

where n is the number of data points.

3.3. Weighting options

Unity weighting, $W_i' = W_i'' = 1.0$

Modulus weighting $W_i' = W_i'' = 1.0/(a_i + b_i)^2$.

According to the literature [26], a χ^2 of the order of 1×10^{-3} or below was acceptable for a given model. The proposed equivalent circuit used for simulating the EIS of the $LaNi_{3.55}Mn_{0.4}Al_{0.3}Co_{0.4}Fe_{0.35}$ alloy electrode, as shown in Fig. 3. In this circuit, R_e is ascribed to the electrolyte resistance, R_{tc} is attributed to the charge-transfer resistance, C_{dl} is the capacitance of the double layer, CPE_{ad} is modeled as constant-phase element replaces the capacitance of the adsorbed (C_{ad}), R_{ab} is the resistance for the hydrogen absorption on the surface of the alloy, R_{ev} is the resistance of the hydrogen evolution process which characterises the parasitic process taking place with the insertion hydrogen in alloys and Z_w is the Warburg impedance for semi-infinite diffusion. Constant phase element (CPE) is used in this circuit model to take into account the porosity, roughness and inhomogeneity of the surface electrode. Thus, capacitance is deduced from the following relation:

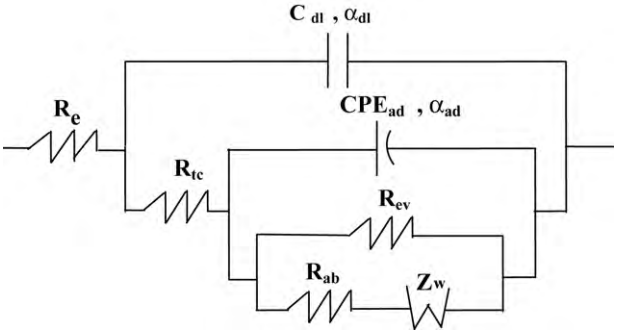

Fig. 3. The proposed equivalent circuit used for simulating the EIS of the $LaNi_{3.55}Mn_{0.4}Al_{0.3}Co_{0.4}Fe_{0.35}$ MH electrode.

$$CPE = Q(\omega_{\max})^{\alpha-1} \quad (4)$$

In this equation, Q is a capacitance parameter, a is a parameter between 0 and 1 and $\omega_{\max} = 2\pi f_{\max}$, where f_{max} represents the frequency at which imaginary value reaches a maximum on the Nyquist plot.

The Warburg diffusion impedance is described by the following equations [27,28]:

$$Z_\omega = \frac{\delta}{\sqrt{\omega}}(1-j) = \frac{RT}{n^2F^2C_0S\sqrt{2\omega}\sqrt{D_H}}(1-j) \quad (5)$$

$$\text{With } \delta = \frac{RT}{n^2F^2SC_0\sqrt{2D_H}} \quad (6)$$

where j is the square root of -1, δ is the Warburg coefficient, n is the number of the exchanged electrons, F is the Faraday constant, S is the geometrical surface of the working electrode (~1 cm^2), C_0 is the concentration of diffusing species (~0.022 mol/cm^3), R is the gas constant, T is the absolute temperature and D_H is the hydrogen diffusion coefficient. Warburg impedance is also defined by

Table 1
Kinetic parameters of the $LaNi_{3.55}Mn_{0.4}Al_{0.3}Co_{0.4}Fe_{0.35}$ metal hydride electrode with state of charge.

Parameters	0% SOC	10% SOC	20% SOC	40% SOC	60% SOC	80% SOC	100% SOC
R_e, $\Omega\,cm^2$	0.39 ± 0.03	0.40 ± 0.03	0.40 ± 0.03	0.39 ± 0.04	0.37 ± 0.04	0.37 ± 0.04	0.36 ± 0.04
R_{tc}, $\Omega\,cm^2$	2.05 ± 0.13	1.76 ± 0.18	1.42 ± 0.18	1.41 ± 0.19	1.36 ± 0.21	1.34 ± 0.23	1.34 ± 0.25
C_{dl}, $\mu F\,cm^{-2}$	76.55 ± 0.50	74.80 ± 0.66	77.90 ± 0.68	77.00 ± 0.69	75.50 ± 0.69	80.20 ± 0.74	84.00 ± 0.81
α_{dl}	1.00 ± 0.02	1.00 ± 0.03	1.00 ± 0.02	1.00 ± 0.02	1.00 ± 0.02	1.00 ± 0.03	1.00 ± 0.02
CPE_{ad}, $mF\,cm^{-2}$	108.63 ± 0.03	125.84 ± 0.06	130.67 ± 0.09	138.66 ± 0.09	138.33 ± 0.09	139.77 ± 0.10	142.96 ± 0.10
α_{ad}	0.72 ± 0.01	0.75 ± 0.03	0.77 ± 0.04	0.78 ± 0.04	0.80 ± 0.04	0.81 ± 0.04	0.81 ± 0.04
Y_0, $S\,s^{1/2}\,cm^{-2}$	0.20 ± 0.01	0.23 ± 0.02	0.32 ± 0.03	0.31 ± 0.02	0.30 ± 0.03	0.30 ± 0.03	0.30 ± 0.03
R_{ab}, $\Omega\,cm^2$	14.63 ± 0.02	9.87 ± 0.03	5.67 ± 0.05	5.56 ± 0.05	5.66 ± 0.05	5.43 ± 0.05	5.56 ± 0.05
R_{ev}, $\Omega\,cm^2$	1.05 ± 0.26	0.99 ± 0.28	0.89 ± 0.25	0.87 ± 0.26	0.90 ± 0.26	0.84 ± 0.30	0.82 ± 0.33
D_H, $10^{-11}\,cm^2\,s^{-1}$	0.57	0.80	1.48	1.38	1.34	1.36	1.33
I_0, mA/g	211.60	245.51	303.03	307.00	317.22	322.42	322.18
I_0/S_r, $mA\,cm^{-2}$	50	59	73.20	73.82	76.47	78.78	78.78
χ^2, 10^{-4}	4.58	1.91	2.13	2.12	2.27	2.38	2.60

the following equation:

$$Z_W = \frac{1}{Y_0(j\omega)^{1/2}} = \frac{1}{\sqrt{2\omega}Y_0}(1-j) \quad (7)$$

where Y_0 is the Warburg admittance, deduced from the fitting of impedance diagrams.

Comparing (5) with (7), we can obtain:

$$\frac{RT}{n^2F^2C_0S\sqrt{2\omega}\sqrt{D_H}} = \frac{1}{\sqrt{2\omega}Y_0} \Rightarrow \frac{RT}{n^2F^2SC_0\sqrt{D_H}} = \frac{1}{Y_0} \quad (8)$$

The hydrogen diffusion coefficient D_H is used to characterize hydrogen diffusion rate in the bulk of alloy. The hydrogen diffusion

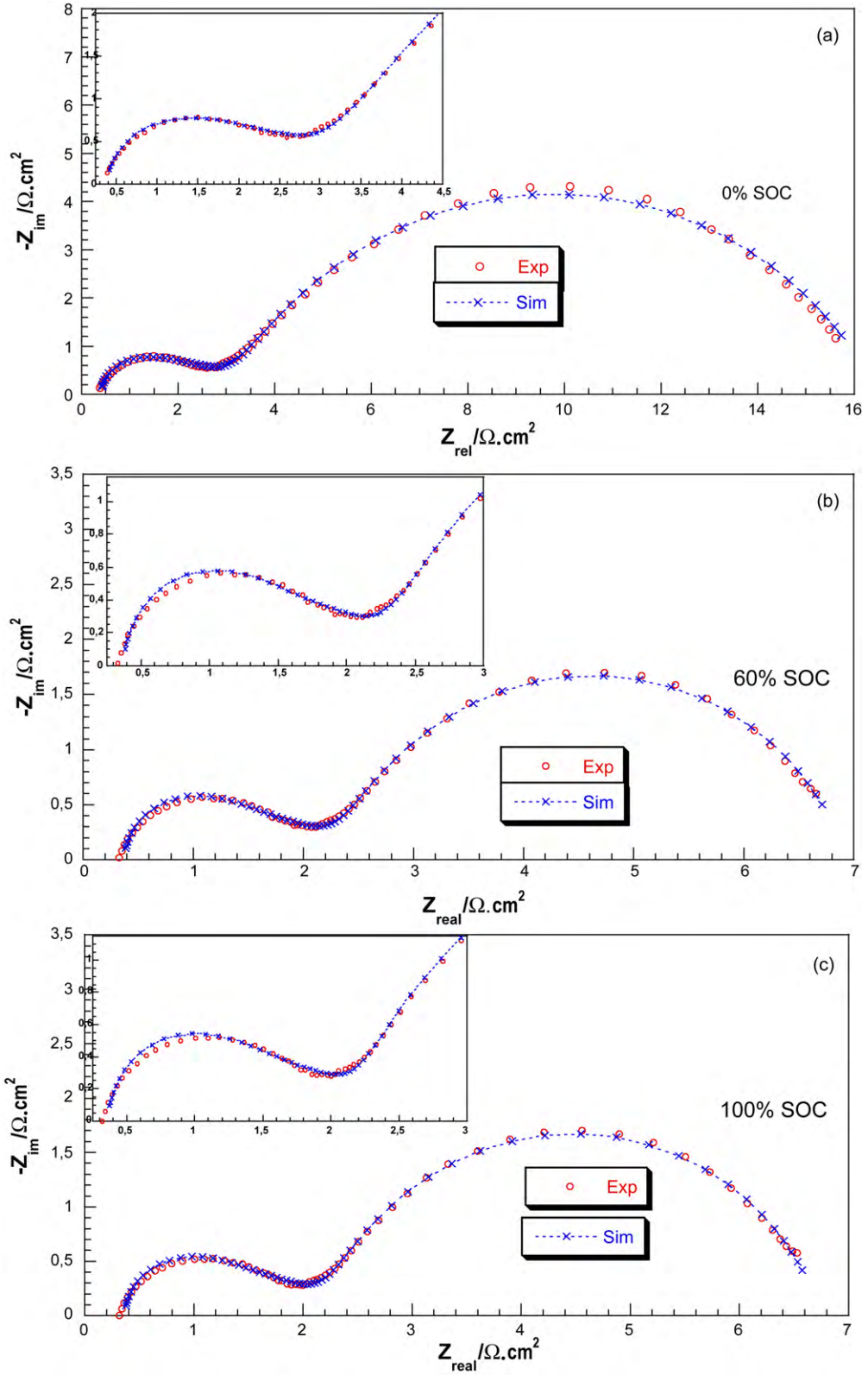

Fig. 4. Nyquist plots and modelling of EIS spectra of the $LaNi_{3.55}Mn_{0.4}Al_{0.3}Co_{0.4}Fe_{0.35}$ electrode with state of charge: (a) 0% SOC; (b) 60% SOC; (c) 100% SOC.

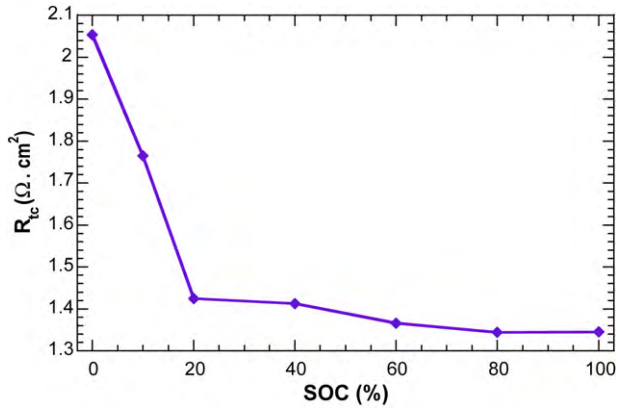

Fig. 5. Charge-transfer resistance of the $LaNi_{3.55}Mn_{0.4}Al_{0.3}Co_{0.4}Fe_{0.35}$ alloy as a function of the state of charge.

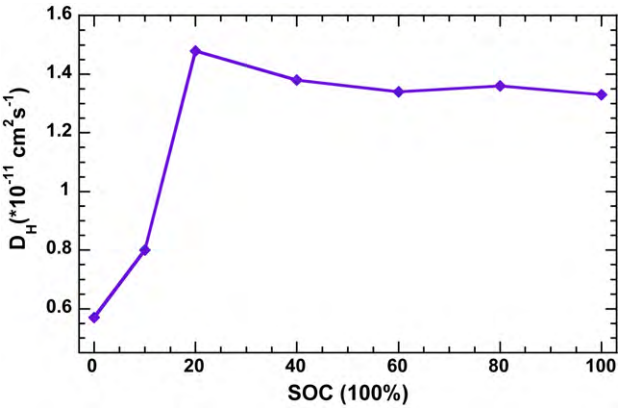

Fig. 7. Hydrogen diffusion coefficient of the $LaNi_{3.55}Mn_{0.4}Al_{0.3}Co_{0.4}Fe_{0.35}$ alloy with different state of charge.

coefficient D_H, can be estimated knowing the Warburg admittance Y_0, deduced from the fitting of impedance diagrams (Eq. (8)):

$$D_H = \left[\frac{RTY_0}{n^2F^2SC_0}\right]^2 \quad (9)$$

The exchange current density I_0, is a powerful parameter for measuring the kinetics of the electrochemical hydrogen reaction, can be estimated by the following formula [29] at the equilibrium potential:

$$I_0 = \left(\frac{RT}{nF}\right)\left(\frac{1}{R_{tc}}\right) \quad (10)$$

where R is the gas constant, n is the number of the exchanged electrons, T is the absolute temperature, F is the Faraday constant and R_{tc} is the charge-transfer resistance. The results of the fitting are shown in Fig. 4(a)–(c). A very high correlation was observed between experimental results and the results calculated with the best fitting electrical equivalent circuit model, where χ^2 was minimized below 10^{-3}. The value parameters of the fitting circuit model are summarized in Table 1.

Fig. 5 shows the variation of the charge-transfer resistance (R_{tc}) as a function of state of charge. When the state of charge of the electrode is less than about 20%, the charge-transfer resistance of the electrode decreases rapidly with hydrogen content. The decrease of the charge-transfer resistance is mainly attributed to the improvement of the surface electrocatalytic activity of the MH electrode. The exchange current density versus the state of charge is shown in Fig. 6. It can be seen that the I_0 value of the alloy electrode increases strongly first from 211.6 mA/g at 0% SOC to 307 mA/g at 40% SOC and then remains almost constant; this implies that the electrochemical reaction activity of the MH electrode is improved with increasing state of charge. Using micropolarization technique, Tafel polarization technique and electrochemical impedance spectroscopy (SIC), Popović et al. [30] found that the exchange current density of the $LaNi_{4.15}Co_{0.43}Mn_{0.40}Fe_{0.02}$ alloy electrode increases with increasing hydrogen concentration in the alloy electrode and the values of the exchange current determined by AC impedance are in good agreement with values obtained by micropolarization and Tafel polarization.

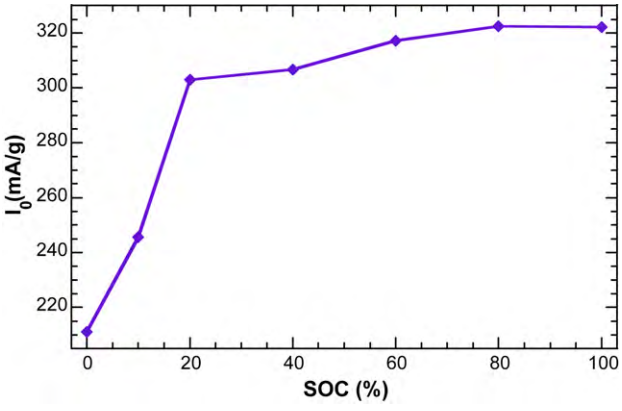

Fig. 6. Exchange current density of the $LaNi_{3.55}Mn_{0.4}Al_{0.3}Co_{0.4}Fe_{0.35}$ alloy as a function of the state of charge.

Fig. 7, presents the hydrogen diffusion coefficient of the alloy electrode at different SOC. It can be seen that the value of the D_H increases rapidly from 0.57×10^{-11} to 1.48×10^{-11} cm^2 s^{-1} with the increase in SOC of the metal hydride electrode from 0 to 20% and then has a maximum value at 40–100% of state of charge. A similar concentration dependence where the diffusion coefficient increases with hydrogen concentration has been seen previously [1,31–35]. The increase in the diffusion coefficient at a low SOC, could be attributed to the change in the crystal structure of the alloy hydride when transforming from the solid solution phase (α phase) to the hydride phase (β phase). The number of vacant sites available for hydrogen to occupy at a low SOC is high compared to that at a high SOC. So the diffusion of hydrogen is influenced not only by its concentration but also by structural change of the metal hydride from the phase α to the phase β at low SOC, but these influences are absent at high SOC. Various authors [36–44] have reported values of hydrogen diffusion coefficient between 10^{-6} and 10^{-14} cm^2 s^{-1} for metal hydride alloys, which agree with our results. Such wide variations in the values for the diffusion coefficient for similar types of alloys could be attributed to variations in the microstructure, metal stoichiometry and composition of the alloys. The microstructure of the alloys depends on their preparation and hydrogenation. The hydrogen diffusion coefficient can also vary with the type of hydrogenation process, i.e. gas-phase hydrogenation/electrochemical hydrogenation [27,44,45].

The values of α_{dl} are equal to 1: give the perfect capacitor of the double layer (Table 1). The C_{dl} values are between 74.80 and 84 μF cm^{-2} (Table 1). These values are in good agreement with those reported in the literature for intermetallic compounds [42,46,47]. The change of the resistance evolution with the state of charge is very small. According to Eq. (4), the CPE_{ad} values of the $LaNi_{3.55}Mn_{0.4}Al_{0.3}Co_{0.4}Fe_{0.35}$ alloy electrode can be estimated and listed in Table 1. It can be seen that the CPE_{ad} values increase from 108.63 mF cm^{-2} at 0% SOC to 142.96 mF cm^{-2} at 100% SOC (Table 1), and R_{ab} changes from 14.63 to 5.56 Ω cm^2 (Table 1), respectively. The variation in the values of the CPE_{ad} could be attributed to surface heterogeneity; due to the variations in the microstructure of

the alloy when transforming from solid solution phase (α phase) to hydride phase (β phase). The values of α_{ad} are different to unity ($\alpha \neq 1$) which causes a strong change of the surface inhomogeneity with increasing SOC (Table 1).

The surface roughness factor of the electrode is estimated from the ratio of the measured double layer capacitance by the EIS and the usual value of the double layer capacitance. Considering the specific double layer capacitance C_{dl} the usual value for metal electrodes is about $C_{dl} = 20\,\mu F\,cm^{-2}$ [48–52], one gets the surface roughness factor, R_f, defined as:

$$R_f = C_{dl}/20\,\mu F\ cm^2 \quad (11)$$

The R_f values are between 3.74 and 4.2. The real surface area, S_r, can be described as:

$$S_r = S \cdot R_f \quad (12)$$

where S is the geometric surface area of the working electrode ($\sim 1\,cm^2$) and R_f is the surface roughness factor. The values of the real surface area, S_r, varied between 3.74 and 4.2 cm^2. This result indicates that the real surface area of the electrode is 4 times larger than the geometric surface area (not equal to 1 cm^2). Taking into account the real surface area of the electrode, the value of the charge-transfer resistance, R_{tc}, is inversely proportional to the active surface area of the electrode. The values of R_{tc} increase from 0.51 Ω cm^2 at 0% SOC to 0.33 Ω cm^2 at 100% SOC and the values of the real exchange current density, I_0/S_r, increase from 50 mA cm^{-2} at 0% SOC to 78.78 mA cm^{-2} at 100% SOC (Table 1).

4. Conclusions

The kinetic properties of the $LaNi_{3.55}Mn_{0.4}Al_{0.3}Co_{0.4}Fe_{0.35}$ metal hydride electrode under different state of charge (SOC) were discussed by electrochemical impedance spectra (EIS). The results show a strong dependence on the electrochemical reaction and the structure transformation of the metal hydride electrode from phase α to phase β (hydrogen concentration). EIS measurements indicate that the kinetic properties of the alloy improved with increasing state of charge, mainly due to the rapidly hydrogen transfer in the bulk of the alloy end the higher electrocatalytic activity of the surface at lower SOC. The transformation α–β is probably a limiting step in the mechanisms of hydrogenation of metal hydride electrode.

References

[1] M. Tliha, H. Mathlouthi, J. Lamloumi, A. Percheron-Guegan, J. Alloys Compd. 436 (2007) 221.
[2] B. Huang, P. Shi, Z. Liang, M. Chen, Y. Guan, J. Alloys Compd. 394 (2005) 303.
[3] X.B. Yu, Z. Wu, T.S. Huang, J. Alloys Compd. 476 (2009) 787.
[4] C.Y. Seo, S.J. Choi, J. Choi, C.Y. Park, P.S. Lee, J.Y. Lee, J. Alloys Compd. 350 (2003) 324.
[5] S. Shi, C. Ouyang, M. Lei, J. Power Sources 164 (2007) 911.
[6] Y. Wang, M. Zhao, S. Li, L. Wang, Electrochem. Acta 53 (2008) 7831.
[7] F. Feng, D.O. Northwood, Int. J. Hydrogen Energy 30 (2005) 1367.
[8] F. Li, K. Young, T. Ouchi, M.A. Fetcenko, J. Alloys Compd. 471 (2009) 371.
[9] P. Zhang, X. Wei, Y. Liu, J. Zhu, Z. Zhang, T. Zhao, J. Alloys Compd. 399 (2005) 270.
[10] J.-Y. Kim, C.-N. Park, J.-S. Shim, C.-Jin. Park, J. Choi, H. Noh, J. Power Sources 180 (2008) 648.
[11] P. Zhang, Y. Liu, J. Zhu, X. Wei, G. Yu, Int. J. Hydrogen Energy 32 (2007) 2488.
[12] J. Ma, H. Pan, Y. Zhu, S. Li, C. Chen, Q. Wang, Electrochem. Acta 46 (2001) 2427.
[13] H. Ye, Y.X. Huang, T.S. Huang, H. Zhang, J. Alloys Compd. 330 (2002) 866.
[14] M.H. Wang, Yao. Zhang, L.Z. Zhang, L.X. Sun, Z.C. Tan, F. Xu, H.T. Yuan, T. Zhang, J. Power Sources 159 (2006) 159.
[15] C. Khaldi, H. Mathlouthi, J. Lamloumi, A. Percheron-Guegan, Int. J. Hydrogen Energy 29 (2004) 307.
[16] M. Tliha, H. Mathlouthi, C. Khaldi, J. Lamloumi, A. Percheron-Guegan, J. Power Sources 160 (2006) 1391.
[17] H. Mathlouthi, J. Lamloumi, M. Latroche, A. Percheron-Guegan, Ann. Chim. Sci. Mater. 22 (1997) 241.
[18] N. Rajalakshmi, K.S. Dhathathreyan, S. Ramaprabhu, Int. J. Hydrogen Energy 26 (2001) 1097.
[19] X. Yuan, N. Xu, J. Alloys Compd. 316 (2001) 113.
[20] C. Wang, J. Electrochem. Soc. 145 (6) (1998) 1801.
[21] H. Yang, Y. Zhang, Z. Zhou, J. Wei, G. Wang, D. Song, X. Cao, C. Wang, J. Alloys Compd. 231 (1995) 625.
[22] R. Baddour-Hadjean, H. Mathlouthi, J.P. Pereira-Ramos, J. Lamloumi, M. Latroche, A. Percheron-Guegan, J. Alloys Compd. 356 (2003) 750.
[23] Y.H. Xu, G.R. He, X.L. Wang, Int. J. Hydrogen Energy 28 (2003) 961.
[24] C. Khaldi, H. Mathlouthi, J. Lamloumi, J. Alloys Compd. 469 (2009) 464.
[25] H. Mathlouthi, C. Khaldi, M. Ben Moussa, J. Lamloumi, A. Percheron-Guegan, J. Alloys Compd. 375 (2004) 297.
[26] X.Y. Cui, D.C. Martin, Sens. Actuators B: Chem. 89 (2003) 92.
[27] X. Yuan, N. Xu, J. Alloys Compd. 329 (2001) 115.
[28] P. Xu, X.J. Han, B. Zhang, Z.S. Lv, X.R. Liu, J. Alloys Compd. 436 (2007) 369.
[29] N. Kuriyama, T. Sakai, H. Miyamura, I. Uehara, H. Ishikawa, J. Alloys Compd. 202 (1993) 183.
[30] M.M. Popović, B.N. Grgur, M.V. Vojnović, P. Rakin, N.V. Krstajić, J. Alloys Compd. 298 (2000) 107.
[31] D. Richter, R. Hemplemann, J. Less-Common Met. 88 (1982) 353.
[32] M. Ciureanu, D.H. Ryan, J.O. Ström-Olsen, M.L. Trudeau, J. Electrochem. Soc. 140 (1993) 579.
[33] J.J. Kim, D.A. Stevenson, J. Non-Cryst. Solids 101 (1988) 187.
[34] H. Miyamura, N. Kuriyama, T. Sakai, K. Oguro, I. Uehara, H. Ishikawa, J. Alloys Compd. 192 (1993) 188.
[35] Z. Zhou, J. Huang, W. Hu, F. Yao, Y. Zhang, J. Alloys Compd. 231 (1995) 297.
[36] F. Cuevas, M. Hirscher, J. Alloys Compd. 313 (2000) 269.
[37] J. Chen, S.X. Dou, D.H. Bradhurst, H.K. Liu, Int. J. Hydrogen Energy 23 (1998) 177.
[38] M. Sato, M. Stange, V.A. Yartys, J. Alloys Compd. 396 (1995) 197.
[39] H.-S. Kim, M. Nishizawa, I. Uchida, Electrochim. Acta 45 (1999) 483.
[40] N. Mani, S. Ramaprabhu, J. Alloys Compd. 363 (2004) 275.
[41] F. Feng, J. Han, M. Geng, D.O. Northwood, J. Electroanal. Chem. 487 (2000) 111.
[42] M. Ben Moussa, M. Abdellaoui, C. Khaldi, H. Mathlouthi, J. Lamloumi, A. Percheron-Guegan, J. Alloys Compd. 399 (2005) 264.
[43] M. Geng, F. Feng, P.J. Sabastian, A.J. Matchett, D.O. Northwood, Int. J. Hydrogen Energy 26 (2000) 165.
[44] F. Feng, J. Han, M. Geng, D.O. Northwood, Int. J. Electroanal. Chem. 487 (2000) 165.
[45] X. Yyan, N. Xu, J. Appl. Electrochem. 31 (2001) 1033.
[46] H. Mathlouthi, J. Lamloumi, A. Percheron-Guegan, R. Baddour, J.P. Pereira, Phys. Chem. News 11 (2003) 54.
[47] C. Khaldi, H. Mathlouthi, J. Lamloumi, A. Percheron-Guegan, Phys. Chem. News 29 (2006) 76.
[48] Z. Kerner, T. Pajkossy, L.A. Kibler, D.M. Kolb, Electrochem. Commun. 4 (2002) 787.
[49] T. Pajkossy, D.M. Kolb, Electrochim. Acta 46 (2001) 3063.
[50] A.M. El-Aziz, R. Hoyer, L.A. Kibler, D.M. Kolb, Electrochim. Acta 51 (2006) 2518.
[51] A.J. Bard, L.R. Faulkner, Electrochimie: Principes, Méthodes et Applications, Maison, Paris, 1983.
[52] C. Hitz, A. Lazia, J. Electroanal. Chem. 532 (2002) 133.